Acta Geochim (2019) 38(4):472–480
https://doi.org/10.1007/s11631-019-00347-9

ORIGINAL ARTICLE

Kyanite far from equilibrium dissolution rate at 0–22 °C and pH of 3.5–7.5

Yilun Zhang[1,4] · Donald J. Rimstidt[2] · Yi Huang[3] · Chen Zhu[1]

Received: 20 April 2019 / Revised: 26 April 2019 / Accepted: 26 April 2019 / Published online: 7 May 2019

Abstract Kyanite is an important and slow-dissolving mineral. Earlier work has measured its dissolution rate at high temperature and acidic pH, but experimental measurements at low temperature and near neutral pH were lacking. The rate equation by Palandri and Kharaka (A compilation of rate parameters of water–mineral interaction kinetics for application to geochemical modeling. US Geological Survey, Open File Report 2004-1068, 2004) indicates that the rate of kyanite dissolution at room temperature and near neutral pH is on the order of 10^{-17} mol m^{-2} s^{-1}, orders of magnitudes slower than most common silicate minerals such as albite and quartz. This study used an externally-stirred mixed-flow reactor, which allows high solid:solution ratios, to measure the dissolution rate of kyanite at 0–22 °C and pH of 3.5–7.5. The measured dissolution rate of kyanite is 4.6–7.6 × 10^{-13} mol m^{-2} s^{-1} at 22 °C, and the apparent activation energy is 73.5 kJ mol^{-1}. This dissolution rate is close to the rate of quartz dissolution and four orders of magnitude faster than the prediction by rate equation of Palandri and Kharaka (2004).

Based on our new experimental data, we recommend the following rate equation for modeling the dissolution of kyanite at ambient temperatures.

$$r = ke^{\frac{-E_a}{R}\left(\frac{1}{T}-\frac{1}{298.15}\right)}$$

where $k = 5.08 \times 10^{-13}$ mol m^{-2} s^{-1}, and $E_a = 73.5$ kJ mol^{-1}. Review of literature data (Carroll in The dissolution behavior of corundum, kaolinite, and andalusite: a surface complex reaction model for the dissolution of aluminosilicate minerals in diagenetic and weathering environs. Dissertation, Northwestern University, 1989) led to a recommended rate equation for andalusite as for $T = 25$ °C and pH = 2–10:

$$r = k_1 a_{H^+}^{n_1} + k_2 + k_3 a_{H^+}^{n_3}$$

where $k_1 = 4.04 \times 10^{-10}$ mol m^{-2} s^{-1}, $k_2 = 7.95 \times 10^{-10}$ mol m^{-2} s^{-1}, $k_3 = 1.01 \times 10^{-17}$ mol m^{-2} s^{-1}, $n_1 = 1.2$ and $n_3 = -0.6$.

Keywords Kinetics · Kyanite · Reaction rates · Mixed-flow reactor

1 Introduction

Kyanite, andalusite, and sillimanite are Al_2SiO_5 polymorphs, which are commonly found in metamorphic rocks. Structurally, kyanite is a nesosilicate, consisting of chains of edge-sharing Al–O octahedrons interlinked by Si–O tetrahedrons and Al–O tetrahedrons. Unlike feldspars, micas and clay minerals, this structure lacks covalent Si–O–Si bonds. As a result, the breaking of Al–O–Al bonds will directly liberate silica directly into solution. The studies of the dissolution kinetics of kyanite, therefore,

✉ Chen Zhu
chenzhu@indiana.edu

[1] Department of Earth and Atmospheric Sciences, Indiana University, Bloomington, IN 47405, USA

[2] Department of Geological Sciences, Virginia Tech, Blacksburg, VA 24061, USA

[3] Department of Geochemistry, Chengdu University of Technology, Chengdu 610059, People's Republic of China

[4] School of Public and Environmental Affairs, Indiana University, Bloomington, IN 47405, USA

provides comparison to other silicate minerals with Si–O–Si bonds.

A few studies have evaluated the dissolution rate of kyanite based on field observations and laboratory experiments. Dryden and Dryden (1946) estimated the weathering rates of three Al_2SiO_5 polymorphs from field observations, based on their relative resistance to weathering. Their results showed that, although kyanite dissolved the fastest among the three polymorphs, it was slower than hornblende, whose field weathering rate is on the order of 10^{-16} mol m^{-2} s^{-1} (White et al. 1996). Oelkers and Schott (1999) carried out a kyanite dissolution experiment at 100–200 °C and pH ~ 2. The dissolution rate at their experimental condition was ~ 10^{-9} to 10^{-10} mol m^{-2} s^{-1}. According to their results, they proposed a rate law (Eq. 1, definitions of the symbols are tabulated in Table 1), where A = 0.2 mol m^{-2} s^{-1}, and E_a = 75 kJ mol^{-1}.

$$r = Ae^{\frac{-E_a}{RT}}\left(\frac{a_{H^+}^3}{a_{Al^{3+}}}\right)^{0.5} \quad (1)$$

Palandri and Kharaka (2004) adopted the experimental results of Oelkers and Schott (1999) and included kyanite in their kinetic database. Figure 1 illustrates the experimental results of Oelkers and Schott (1999) and the rate equation proposed by Palandri and Kharaka (2004). The extrapolation extends over seven orders of magnitudes from ~ 150 °C and pH ~ 2 to 25 °C and pH ~ 7. Due to the large gap between the experimental condition and the weathering condition in terms of pH and temperature the validity of this extrapolation is questionable. The dissolution rate at low temperature and near-neutral pH calculated from the equation of Palandri and Kharaka (2004) is ~ 10^{-17} mol m^{-2} s^{-1} (Fig. 1). Such a slow rate at near neutral pH is several orders of magnitudes slower than any known dissolution rate of silicate minerals, even compared to very resistant minerals such as quartz and kaolinite (Palandri and Kharaka 2004; Marini 2006; Brantley 2008).

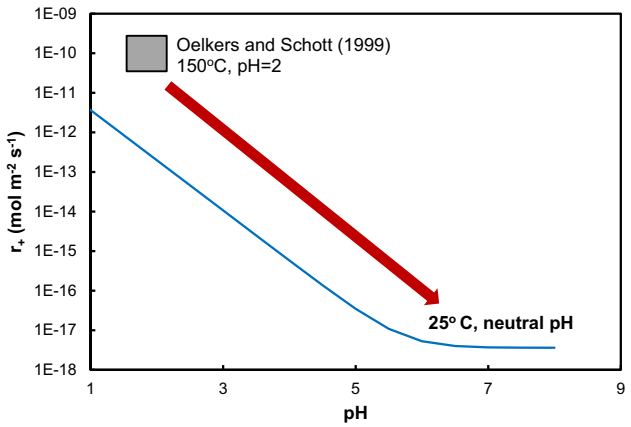

Fig. 1 Dissolution rates of kyanite measured by Oelkers and Schott (1999) at high temperature and acidic pH (shaded area), and the extrapolated dissolution rate by Palandri and Kharaka (2004) to room temperature (blue curve). The extrapolation was over a wide range of pH and temperature

Such slow rates also cannot be measured by the conventional experimental method (Ganor et al. 2007).

In this study, we endeavored to fill the data gap and measure the dissolution rate of kyanite at low temperature and near-neutral pH. As the rate is potentially slow, an externally-stirred column reactor, which is capable of holding a large solid to solution ratio, was used. This enables the measurement of the slow dissolution rate of kyanite at room temperature and near-neutral pH.

2 Method

2.1 Materials

A crushed kyanite sample (in 200 mesh size, from Buckingham, VA) was purchased from Virginia Kyanite. The powder was sieved to obtain a 53–74 μm portion (200–270 mesh). XRD analysis showed the samples contain 90%

Table 1 Experimental conditions and solution chemistry of the effluent for all experiments

ID	Influent pH at 25 °C	Flow rate (mL h^{-1})	Temp (°C)	Steady-state effluent		
				In situ pH	[Si] (μM)	[Al] (μM)
KY1	5.52	1.76	22	6.44	10.3	N.D.[a]
KY2	4.00	1.45	22	4.69	12.7	7.2
KY3	9.99	1.61	22	7.48	7.6	N.D.[a]
KY4	11.24	1.69	22	7.56	8.4	N.D.[a]
KY5	3.09	1.58	22	3.23	7.9	17.8
KYLT1	5.50	0.61	0	4.84	1.8	3.4
KYLT2	10.28	0.60	0	7.30	1.4	N.D.[a]
KYHT1	4.40	0.58	0	5.15	1.1	0.2
KYHT2	3.60	0.61	0	4.68	2.5	19.2[b]

[a]Below detection limit (5 ppb, or 0.19 μM)

[b]Steady state not achieved. Last sample point was used

kyanite, 9% quartz, and 1% rutile. The initial specific surface area of the kyanite powder was characterized with N_2-BET measurements, yielding an initial BET surface area of 0.461 $m^2\ g^{-1}$. The sieved powder was first ultra-sonicated and rinsed with ethanol three times for 10 min per treatment to remove submicron-to-micron sized particles. Next, the ultra-sonicated powder was rinsed with ethanol $\sim$ 10 times until the supernatant was clear, and then air-dried overnight.

To further reduce the "highly-reactive sites" on the surface, the cleaned powder was immersed in DI water in HDPE bottles. The bottles were maintained at 80 °C in a water bath for 6 weeks. After that, the water was decanted and the powder was rinsed with ethanol three times to remove the residue water. The pre-treated kyanite powder was air-dried overnight and kept in a desiccator for the experiment. The pre-treated kyanite samples were also characterized by SEM analysis. The result shows that the samples were nearly free of ultrafine particles and the crystal surfaces were mostly fresh (Fig. 2).

2.2 Externally-stirred mixed flow reactor

An externally-stirred column reactor was used for this experiment (Rimstidt et al. 2016, see Fig. 3). This reactor uses a densely-packed column made of PVC instead of a continuously stirred tank, and it uses a fast and turbulent flow to ensure efficient mixing. The packed-column design allows for a very large solid to solution ratio ($\sim$ 1 g/L mL in this experiment), compared to the common tank reactor (usually $<$ 1 g/10 mL). As a result, the externally-stirred column reactor is better suited for running kinetic experiments involving minerals with very slow reaction rates. Two cotton balls were placed at the ends of the column, to prevent the particles from being flushed out. The column was sealed by two rubber stoppers and epoxy resin. Continuous fast mixing was achieved via a recycle pump that purged the solution through the column at a high flow rate, which reduced the concentration gradient inside the column. A gas wash bottle was installed before the influent storage tank to prevent the atmospheric CO_2 from decreasing the pH of the influent.

For this kyanite experiment, the column was 10 cm in length, 1.5 cm in diameter, and it held $\sim$ 20 g of pre-treated kyanite. The flow rate of the feeding pump was adjusted to 0.5–10 mL h^{-1}, according to the reaction rate of kyanite at the experimental conditions. The recycle pump ran at a much higher flow rate ($>$ 100 mL h^{-1}). The influent solution was 1 mM $NaNO_3$ solution. The initial pH of the influent was adjusted within the range of 3–11, using with concentrated HNO_3 and NaOH solutions. No pH buffers were used in this experiment. The experiments were carried out at room temperature (22 °C) and 0 °C (temperature controlled by an ice bath).

The dissolution rate was calculated by measuring the change in effluent concentration through Eq. (2) at steady state. Since the concentration of Al could be decreased by Al hydroxide precipitation and cause interference on rate determination, Si was used as the reaction progress variable for estimating the dissolution rate of kyanite according to the following formula:

$$r = \frac{Q[\mathrm{Si}]_{\mathrm{out}}}{vm \cdot SSA} \tag{2}$$

2.3 Sample collection and analysis

10 mL of samples were collected each day for each experiment. At the start and end of the collection process,

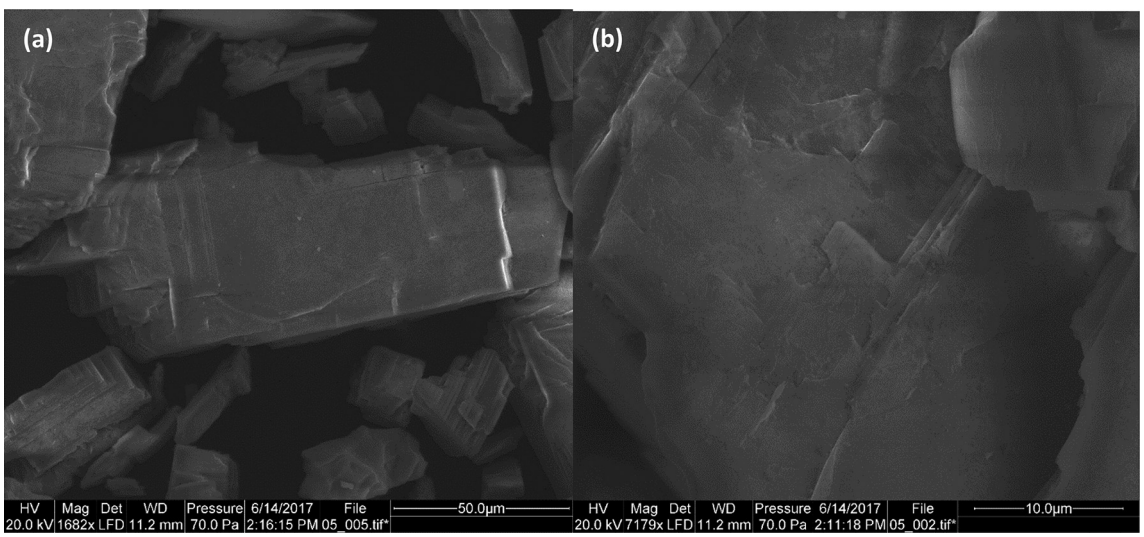

Fig. 2 **a** SEM micrographs of treated kyanite samples, **b** is a zoom-in view of the kyanite sample surface

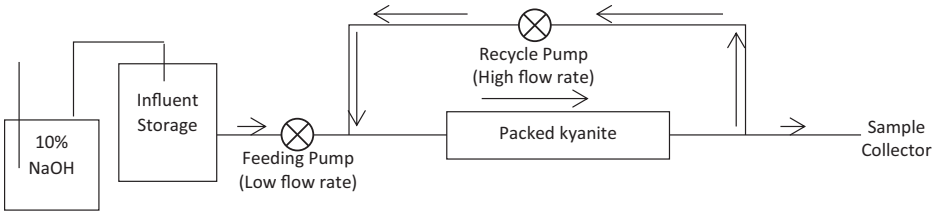

Fig. 3 Schematic illustration of the externally-stirred mixed flow reactor

the time was recorded and the mass of the collectors was measured. The flow rate of the feeding pump was then calculated as the ratio of the change in collector mass to the change in time. The collected samples were subsequently separated into two portions: one for pH and Si concentration analysis and the other for Al analysis. The Al portion was then immediately acidified with concentrated HCl to avoid Al precipitation. In the the pH/Si portion, pH was also measured immediately after sample collection (an exception was made in the case of experiments at 0 °C, for which pH was measured when the solution had equilibrated to room temperature). Each experiment ran until steady-state was achieved. In this study, the steady state is defined as three to five consecutive samples whose Si concentrations varied by less than 10% (Yang and Steefel 2008; Gudbrandsson et al. 2014).

Total concentrations of dissolved Si in solution were analyzed with a Perkin Elmer Lambda 2S UV–visible spectrophotometer, using the molybdate blue method (Govett 1961). The uncertainty in measured Si was less than ± 5% for concentrations above 4 μM. Total [Al] were analyzed via ICP-MS with a measurement uncertainty of ± 5%. The detection limit of this method is estimated to be 5 ppb (∼ 0.2 μM). In this study, we define the uncertainty as the 95% confidence interval.

2.4 Thermodynamic properties and calculations

Standard state thermodynamic properties for most end-member minerals were taken from Holland and Powell (2011). For allophane and imogolite, the thermodynamic properties were re-calculated based on the recommendations of Su and Harsh (1994, 1998) and Stefansson and Gíslason (2001), in order to ensure that they were internally consistent with the rest of SUPCRTBL database (Zimmer et al. 2016). For Al-bearing aqueous species, the thermodynamic properties were taken from Tagirov and Schott (2001); for SiO_2^o(aq), they were taken from Rimstidt (1997) and Apps and Spycher (2004); for the rest of the aqueous species, they were taken from Shock and Helgeson (1988), Shock et al. (1989, 1997), and Sverjensky et al. (1997). When applicable, the T and P dependencies of the thermodynamic properties for aqueous species were predicted using the parameters of the revised HKF equations of state for aqueous species (Helgeson et al. 1981; Tanger and Helgeson 1988; Shock et al. 1992).

The equilibrium constants of relevant reactions were calculated through SUPCRTBL (Zimmer et al. 2016), using the heat capacity function of Holland and Powell (2011) for minerals. Speciation and solubility calculations were performed by PHREEQC 3.4 (Parkhurst and Appelo 2013). A customized database compatible with PHREEQC at 0.01–90 °C and 1 bar using the above-mentioned equilibrium constants was constructed specifically for this modeling study. Activity coefficients for the charged aqueous species were calculated from B-dot equation fitted to mean salt NaCl activity coefficients (Helgeson et al. 1978; Oelkers and Helgeson 1990). Activity coefficients for neutral or uncharged aqueous species were calculated from the Setchénow equation with a coefficient of 0.1 (PHREEQC).

In evaluating the aqueous speciation and mineral saturation states at experimental conditions, we used the pH and total analytical concentrations of the constituents measured at ambient conditions (i.e. ∼ 22 °C and 1 bar) as inputs for the modeling codes and then "re-heated" the solution to experimental T and P. This method calculates the in situ pH at the experimental conditions by taking account of the effects of T and P on the distribution of aqueous species (Zhu et al. 2010).

3 Results

3.1 Al:Si stoichiometry

The experimental conditions and solution chemistry of the effluent in all the experiments are tabulated in Table 1. The typical temporal evolution curves of the effluent Si concentration and pH are shown in Fig. 4. Since there is no buffer in the influent solution, the pH of the effluent was shifted over time as the kyanite dissolution reaction consumed or released H^+ (Fig. 4b), depending on the solution pH (Eqs. 3–7).

$$Al_2SiO_5 + 6H^+ \rightleftharpoons 2Al^{3+} + H_4SiO_4^o + H_2O \quad (3)$$

$$Al_2SiO_5 + 4H^+ + H_2O \rightleftharpoons 2Al(OH)^{2+} + H_4SiO_4^o \quad (4)$$

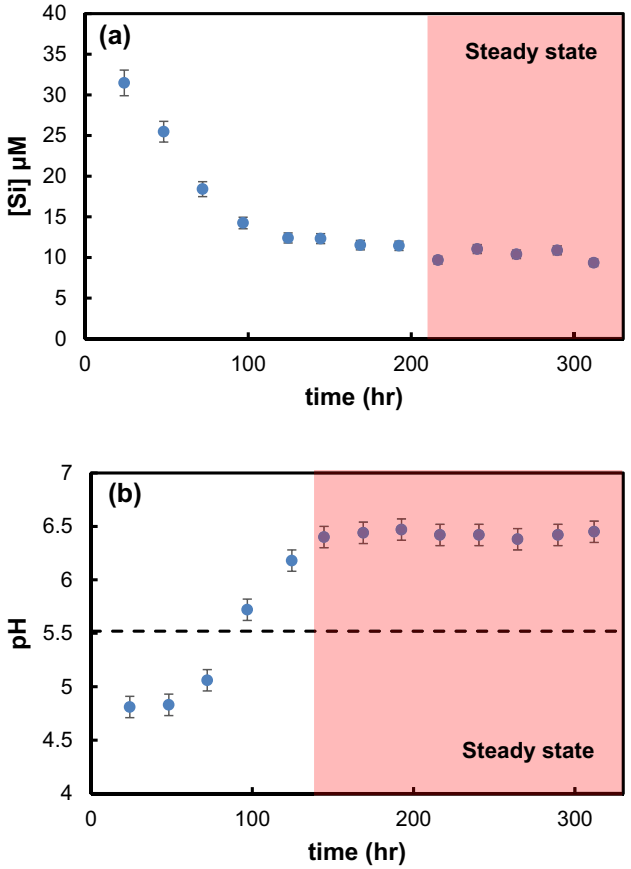

Fig. 4 An example of the temporal evolution of Si concentration (**a**) and pH (**b**) in a kyanite dissolution experiment at 22 °C (KY1). The influent pH in this experiment is 5.52 (denoted as a dashed line). Shaded area denotes the steady state observed in this experiment. Al concentration in the KY1 experiment was below the detection limit and thus not shown. Error bars stand for the 95% confidence interval (± 5% for Si concentration and ± 0.1 for pH measurement)

$$Al_2SiO_5 + 2H^+ + 3H_2O \rightleftharpoons 2Al(OH)_2^+ + H_4SiO_4^o \quad (5)$$

$$Al_2SiO_5 + 5H_2O \rightleftharpoons 2Al(OH)_3^o + H_4SiO_4^o \quad (6)$$

$$Al_2SiO_5 + 7H_2O \rightleftharpoons 2Al(OH)_4^- + H_4SiO_4^o + 2H^+ \quad (7)$$

As Table 1 shows, a number of experiments had low Al concentrations and several were below the detection limit, especially at near-neutral pH (Fig. 5). The dissolution of kyanite was congruent when the pH was low, but the dissolution was incongruent near neutral pH (Fig. 6). The Al:Si ratio was far less than the theoretical stoichiometric ratio of 2 in the near-neutral pH range. An exception to this trend was the KYHT2 experiment in which the Al concentration never achieved a steady state (and thus was not shown in Fig. 6). Figure 5 shows the solubility of gibbsite at various temperatures and pH levels. At near-neutral pH, Al concentration was below the detection limits and could be regulated by gibbsite solubility (Fig. 5).

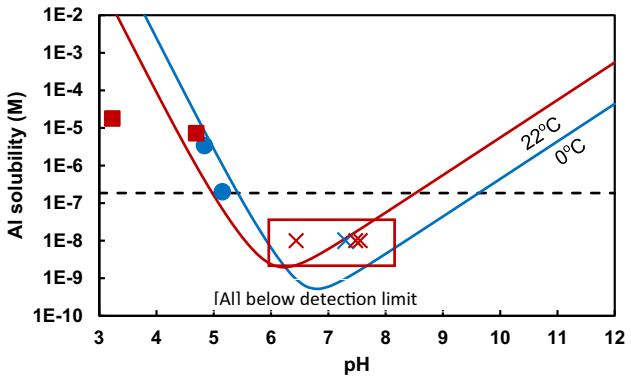

Fig. 5 Aluminum solubility at different pH values, assuming dissolved Al is at equilibrium with gibbsite. The dashed line is the common detection limit of Al concentrations by an ICP-MS. Solid symbols represent the Al concentrations measured in the experiments; cross symbols represent the sample pH but without measurable Al concentrations. Red notation stands for the 22 °C experiments, and blue notation stands for the 0 °C experiments. The red box denotes the experiments where Al concentrations are below detection limits. The KYHT2 experiment is not shown on this figure because steady state effluent concentration for Al was not achieved during the experiment

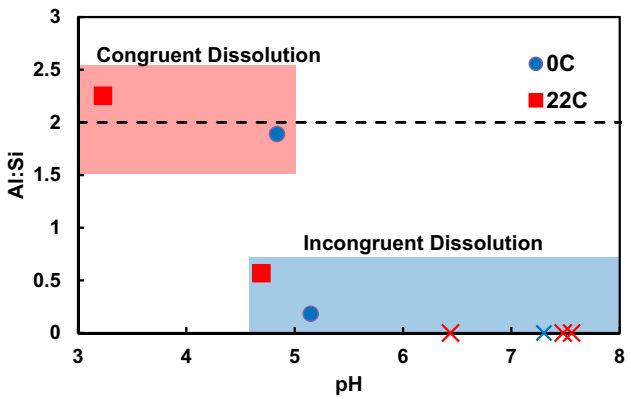

Fig. 6 The Al:Si ratios in the effluent. Symbols represent the steady state Al:Si ratio in each experiment (0 °C experiments denoted as blue circles and 22 °C experiments denoted as red squares. Solid symbols represent ICP-MS measurements, cross symbols represent ratios calculated with assumed [Al] concentrations that is at equilibrium with gibbsite. The dashed line is the theoretical stoichiometric ratio in kyanite. The KYHT2 experiment is not shown on this figure because steady state effluent concentration for Al was not achieved during the experiment

3.2 Saturation indices of the effluent

Saturation indices (SI) for kyanite and common secondary phases were calculated for the steady-state effluent of each experiment (Table 2). For those experiments in which the Al concentration was below detection, Al concentration was assumed to be at equilibrium with gibbsite.

The calculated SI for kyanite was mostly much less than − 2.1, within the range defined as far from equilibrium

(Rimstidt 2014). The calculated SIs for kaolinite showed that the effluent was undersaturated with respect to kaolinite for 0 °C experiments, and slightly supersaturated for 22 °C experiments. With respect to allophane and other intermediate secondary phases (e.g., imogolite and halloysite), the effluent was undersaturated in every experiment. (In the interest of brevity, the SI calculation of the other intermediate secondary phases are not presented in this paper.)

3.3 Kyanite dissolution rate

The dissolution rates were calculated using Eq. (2) based on Si concentrations, and are tabulated in Table 3. At room temperature, the measured dissolution rate of kyanite was $5–8\times10^{-13}$ mol m^{-2} s^{-1}. This rate is similar to that of quartz, slightly slower than feldspars, and much slower than pyroxene and olivine (Fig. 7). This result agrees with the field observation that kyanite is resistant to weathering (Dryden and Dryden 1946; Velbel 1999). Furthermore, the dissolution of kyanite showed little dependence on the solution pH. This is in contrast with the strong pH dependence of dissolution rates for most silicate minerals (Fig. 7).

Figure 8 shows the dissolution rates measured in experiments as a function of pH. Unlike most aluminosilicates, whose dissolution rates are strongly correlated with pH, kyanite's dissolution rate is approximately constant over a wide range of pH. This trend has also been observed for andalusite (Carroll 1989), whose dissolution rate is also almost constant over the pH range of 2–10. To our knowledge, this phenomenon is unusual for silicate minerals, and it might be attributed to the mineral structure of the Al_2SiO_5 polymorphs.

The activation energy of the kyanite dissolution reaction was estimated by comparing the dissolution rate at temperatures of 0 °C and 22 °C using the Arrhenius equation (Eq. 8). The calculated activation energy in this study was 73.5 kJ mol^{-1}, close to the activation energy of 75 kJ mol^{-1} proposed by Oelkers and Schott (1999) based on the rate differences between 111 and 150 °C. The activation energy measured in this experiment falls within the range for most silicate minerals (Palandri and Kharaka 2004; Brantley 2008).

$$\log r = \log A - \frac{E_a}{2.303RT} \quad (8)$$

4 Discussion

4.1 Al inhibition effect and the Palandri and Kharaka rate at 25 °C

Prior to this study, kyanite dissolution rates had not been measured at low temperatures and non-acidic pH. Palandri and Kharaka (2004) extrapolated the rate constant for kyanite from high temperature to low temperature and acidic pH to near neutral pH based on the experimental data of Oelkers and Schott (1999). Their extrapolated rate constant for the neutral mechanism (k_{H2O} at 25 °C) is $10^{-17.44}$ mol m^{-2} s^{-1}, which is $\sim$ 5 orders of magnitudes lower than the dissolution rate of kyanite that we measured at room temperature and near neutral pH. This huge discrepancy appears to be the result of their improper assumption of a constant Al concentration while applying the Al inhibition model of Oelkers and Schott (1999). At near-neutral pH, the Al concentration is most likely regulated by the solubility of gibbsite or other Al-bearing phases (Fig. 5). Therefore, the assumption that Al

Table 2 The saturation indices of kyanite and kaolinite in the effluent of all the experiments

ID	Influent pH at 25 °C	Temp (°C)	Steady-state effluent				
			In situ pH	SI (ky)	SI (kln)	SI (gbs)	SI (allophane-1.64)
KY1	5.52	22	6.44	− 3.4[a]	0.5[a]	0[a]	− 1.8[a]
KY2	4.00	22	4.69	− 1.8	2.2	0.8	− 0.2
KY3	9.99	22	7.48	− 3.5[a]	0.2[a]	0[a]	− 2.0[a]
KY4	11.24	22	7.56	− 3.5[a]	0.3[a]	0[a]	− 1.9[a]
KY5	3.09	22	3.23	− 9.8	− 6.0	− 3.1	− 8.2
KYLT1	5.50	0	4.84	− 5.3	− 1.2	− 0.4	− 3.7
KYLT2	10.28	0	7.30	− 4.5[a]	− 0.5[a]	0[a]	− 3.0[a]
KYHT1	4.40	0	5.15	− 4.6[a]	− 0.8[a]	0[a]	− 3.1[a]
KYHT2	3.60	0	4.68	− 4.6	− 0.4	− 0.2	− 3.0

[a]Using the assumption of gibbsite saturation

Table 3 Calculated dissolution rates for kyanite

ID	Influent pH at 25 °C	Flow rate (mL h^{-1})	Temperature (°C)	In situ pH	Kyanite dissolution rate (mol m^{-2} s^{-1})
KY1	5.52	1.76	22	6.44	6.1×10^{-13}
KY2	4.00	1.45	22	4.69	7.6×10^{-13}
KY3	9.99	1.61	22	7.48	5.0×10^{-13}
KY4	11.24	1.69	22	7.56	5.8×10^{-13}
KY5	3.09	1.58	22	3.23	4.6×10^{-13}
KYLT1	5.50	0.61	0	4.84	2.7×10^{-14}
KYLT2	10.28	0.60	0	7.30	3.4×10^{-14}
KYHT1	4.40	0.58	0	5.15	2.8×10^{-14}
KYHT2	3.60	0.61	0	4.68	2.9×10^{-14}

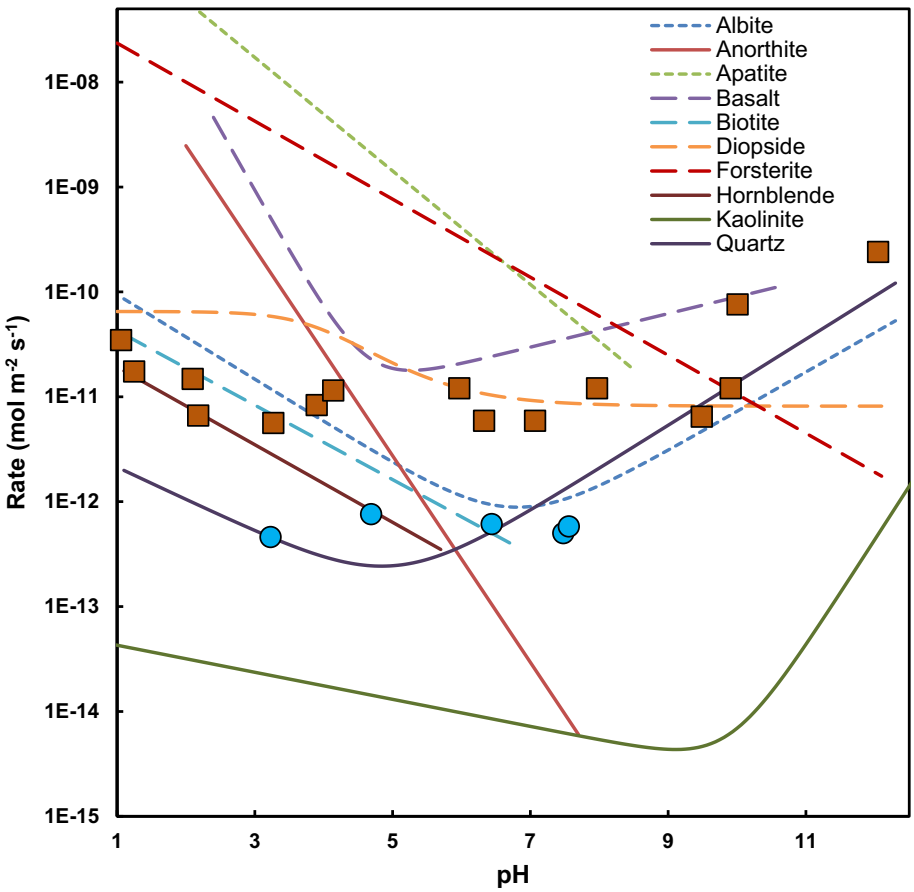

Fig. 7 Comparison of the dissolution rates of kyanite and andalusite with other minerals at 25 °C. Blue circles represent the measured dissolution rates of kyanite from this study at 22 °C, and red squares represent the andalusite dissolution rate from Carroll (1989) at 25 °C. The dissolution rates of other minerals were calculated following Brantley (2008)

concentration over a wide pH range is constant was not appropriate.

4.2 Proposed rate equations for kyanite and andalusite dissolution

We recommend a rate equation to replace the rate equation proposed by Palandri and Kharaka (2004) because of the errors in their extrapolation of rates from acidic to neutral pH range. This rate equation works for the pH range of 3.5–7.5 and T = 0–22 °C, and is written as

$$r = ke^{\frac{-E_a}{R}\left(\frac{1}{T}-\frac{1}{298.15}\right)} \quad (9)$$

where $k = 5.08 \times 10^{-13}$ mol m^{-2} s^{-1}, and $E_a = 73.5$ kJ mol^{-1}.

The rate equation for andalusite at 25 °C and for the pH range of 2–10 is based on the experimental data from Carroll (1989), and is given by

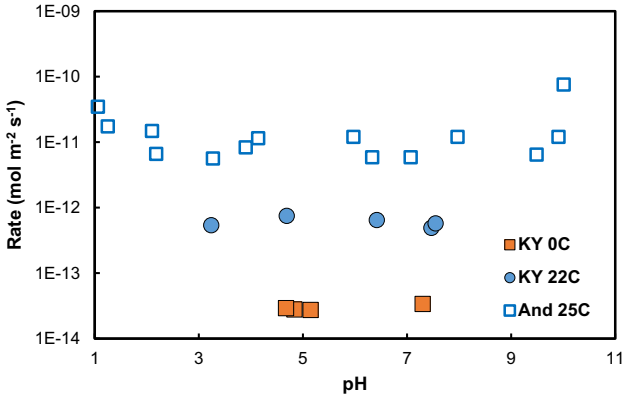

Fig. 8 Kyanite dissolution rates at various pH and temperatures (solid symbols). Andalusite dissolution rates from Carroll (1989) at various pH at 25 °C and 80 °C (open symbols) were also plotted for comparison

$$r = k_1 a_{H^+}^{n_1} + k_2 + k_3 a_{H^+}^{n_3} \quad (10)$$

where $k_1 = 4.04 \times 10^{-10}$ mol m^{-2} s^{-1}, $k_2 = 7.95 \times 10^{-10}$ mol m^{-2} s^{-1}, $k_3 = 1.01 \times 10^{-17}$ mol m^{-2} s^{-1}, $n_1 = 1.2$ and $n_3 = -0.6$.

5 Conclusions

In this study, mixed reactor experiments were carried out to measure kyanite dissolution rates at low temperatures (0–22 °C) and pH of 3.5–7.5, at far-from-equilibrium conditions. Dissolution is nearly stoichiometric in acidic conditions (pH < 4.5), but becomes non-stoichiometric at higher pH (pH > 4.5), probably due to the precipitation of Al-hydroxide phases. The dissolution rate of kyanite at room temperature is 5–8 × 10^{-13} mol m^{-2} s^{-1} at pH = 3.5–7.5, which is much slower than most common silicate minerals and is similar to quartz. The activation energy of kyanite dissolution reaction is 73.5 kJ mol^{-1}. The dissolution rate of kyanite at room temperature is also slower than the rate of andalusite in Carroll (1989), contrary to the prediction in Dryden and Dryden (1946).

We propose a new rate equation for kyanite based on our experimental data to replace the dissolution rate equation for kyanite proposed by Palandri and Kharaka (2004). The latter is the result of an extrapolation from acidic pH to neutral pH under the improper assumption of constant total Al concentration. These extrapolated rates are five orders of magnitude slower than those which we observed in our experiments. We also propose a new rate equation for andalusite based on experimental data found in the literature.

These new rate equations were programmed into Basic language scripts that are suitable to be used in the United State Geological Survey geochemical modeling software PHREEQC (Parkhurst and Appelo 2013) and can be downloaded from the website of www.indiana.edu/~hydrogeo.

Acknowledgements Financial support of this research was provided by the U.S. NSF Grant EAR-1225733 to Dr. Chen Zhu, and Indiana University.

References

Apps J, Spycher N (2004) Data qualification for thermodynamic data used to support THC calculations. ANL-NBS-HS-000043 REV 00, Bechtel SAIC Company, LLC, Las Vegas, NV. DOC.20041118.0004

Brantley SL (2008) Kinetics of mienral dissolution. In: Brantley SL, Kubicki JD, White AF (eds) Kinetics of water–rock interaction. Springer, New York, pp 151–210

Carroll SA (1989) The dissolution behavior of corundum, kaolinite, and andalusite: a surface complex reaction model for the dissolution of aluminosilicate minerals in diagenetic and weathering environs. Dissertation, Northwestern University

Dryden L, Dryden C (1946) Comparative rates of weathering of some common heavy minerals. J Sediment Res 16:91–96

Ganor J, Lu P, Zheng Z, Zhu C (2007) Bridging the gap between laboratory measurements and field estimations of silicate weathering using simple calculations. Environ Geol 53:599–610

Govett G (1961) Critical factors in the colorimetric determination of silica. Anal Chim Acta 25:69–80

Gudbrandsson S, Wolff-Boenisch D, Gislason SR, Oelkers EH (2014) Experimental determination of plagioclase dissolution rates as a function of its composition and pH at 22 °C. Geochim Cosmochim Acta 139:154–172

Helgeson HC, Delany JM, Nesbitt HW, Bird DK (1978) Summary and critique of the thermodynamic behavior of aqueous electrolytes at high pressure and temperature. Am J Sci 787:1–229

Helgeson HC, Kirkham DH, Flowers GC (1981) Theoretical prediction of the thermodynamic behavior of aqueous electrolytes by high pressures and temperatures; IV, Calculation of activity coefficients, osmotic coefficients, and apparent molal and standard and relative partial molal properties to 600 degrees C and 5kb. Am J Sci 281:1249–1516

Holland T, Powell R (2011) An improved and extended internally consistent thermodynamic dataset for phases of petrological interest, involving a new equation of state for solids. J Metamorph Geol 29:333–383

Marini L (2006) Geological sequestration of carbon dioxide: thermodynamics, kinetics, and reaction path modeling. Elsevier, Amsterdam

Oelkers EH, Helgeson HC (1990) Triple-ion anions and polynuclear complexing in supercritical electrolyte solutions. Geochim Cosmochim Acta 54:727–738

Oelkers EH, Schott J (1999) Experimental study of kyanite dissolution rates as a function of chemical affinity and solution composition. Geochim Cosmochim Acta 63:785–797

Palandri JL, Kharaka YK (2004) A compilation of rate parameters of water–mineral interaction kinetics for application to geochemical modeling. US Geological Survey, Open File Report 2004-1068

Parkhurst DL, Appelo C (2013) Description of input and examples for PHREEQC version 3—a computer program for speciation, batch-reaction, one-dimensional transport, and inverse

geochemical calculations. US geological survey techniques and methods, book 6, 497

Rimstidt JD (1997) Quartz solubility at low temperatures. Geochim Cosmochim Acta 61:2553–2558

Rimstidt JD (2014) Geochemical Rate models: an introduction to geochemical kinetics. Cambridge University Press, Cambridge

Rimstidt JD, Zhang Y, Zhu C (2016) Rate equations for sodium catalyzed amorphous silica dissolution. Geochim Cosmochim Acta 195:120–125

Shock EL, Helgeson HC (1988) Calculation of the thermodynamic and transport properties of aqueous species at high pressures and temperatures: correlation algorithms for ionic species and equation of state predictions to 5 kb and 1000 °C. Geochim Cosmochim Acta 52:2009–2036

Shock EL, Helgeson HC, Sverjensky DA (1989) Calculation of the thermodynamic and transport properties of aqueous species at high pressures and temperatures: standard partial molal properties of inorganic neutral species. Geochim Cosmochim Acta 53:2157–2183

Shock EL, Oelkers EH, Johnson JW, Sverjensky DA, Helgeson HC (1992) Calculation of the thermodynamic properties of aqueous species at high pressures and temperatures. Effective electrostatic radii, dissociation constants and standard partial molal properties to 1000 °C and 5 kbar. J Chem Soc Faraday Trans 88:803–826

Shock EL, Sassani DC, Willis M, Sverjensky DA (1997) Inorganic species in geologic fluids: correlations among standard molal thermodynamic properties of aqueous ions and hydroxide complexes. Geochim Cosmochim Acta 61:907–950

Stefansson A, Gíslason SR (2001) Chemical weathering of basalts, Southwest Iceland: effect of rock crystallinity and secondary minerals on chemical fluxes to the ocean. Am J Sci 301:513–556

Su C, Harsh JB (1994) Gibbs free energies of formation at 298 K for imogolite and gibbsite from solubility measurements. Geochim Cosmochim Acta 58:1667–1677

Su CM, Harsh JB (1998) Dissolution of allophane as a thermodynamically unstable solid in the presence of boehmite at elevated temperatures and equilibrium vapor pressures. Soil Sci 163:299–312

Sverjensky DA, Shock EL, Helgeson HC (1997) Prediction of the thermodynamic properties of aqueous metal complexes to 1000 °C and 5 kb. Geochim Cosmochim Acta 61:1359–1412

Tagirov B, Schott J (2001) Aluminum speciation in crustal fluids revisited. Geochim Cosmochim Acta 65:3965–3992

Tanger JC, Helgeson HC (1988) Calculation of the thermodynamic and transport properties of aqueous species at high pressures and temperatures; revised equations of state for the standard partial molal properties of ions and electrolytes. Am J Sci 288:19–98

Velbel MA (1999) Bond strength and the relative weathering rates of simple orthosilicates. Am J Sci 299:679–696

White A, Blum AE, Schulz MS, Bullen TD, Harden JW, Peterson ML (1996) Chemical weathering rates of a soil chronosequence on granitic alluvium: I. Quantification of mineralogical and surface area changes and calculation of primary silicate reaction rates. Geochim Cosmochim Acta 60:2533–2550

Yang L, Steefel CI (2008) Kaolinite dissolution and precipitation kinetics at 22 °C and pH 4. Geochim Cosmochim Acta 72:99–116

Zhu C, Lu P, Zheng Z, Ganor J (2010) Coupled alkali feldspar dissolution and secondary mineral precipitation in batch systems: 4. Numerical modeling of kinetic reaction paths. Geochim Cosmochim Acta 74:3963–3983

Zimmer K, Zhang Y, Lu P, Chen Y, Zhang G, Dalkilic M, Zhu C (2016) SUPCRTBL: a revised and extended thermodynamic dataset and software package of SUPCRT92. Comput Geosci 90:97–111